applied optics

Temporal characterization of petawatt class laser at Shen Guang II facility

Xiaoping Ouyang,[1,*] Yong Cui,[2] Jian Zhu,[2] Baoqiang Zhu,[1] and Jianqiang Zhu[1]

[1]Joint Laboratory on High Power Laser and Physics, Shanghai Institute of Optics and Fine Mechanics, Chinese Academy of Sciences, Shanghai 201800, China
[2]Shanghai Institute of Laser Plasma, China Academy of Engineering Physics, Shanghai 201800, China
*Corresponding author: oyxp@siom.ac.cn

Received 11 July 2016; revised 19 August 2016; accepted 19 August 2016; posted 22 August 2016 (Doc. ID 270279); published 14 September 2016

Temporal characterization is important to diagnose and measure a petawatt (PW) class laser. We obtained the V curve of the pulse width versus the grating position using pulse width measurement with a mirror image configuration. The temporal range for pulse width was 18 ps with a resolution of 0.05 ps. We measured the pulse contrast between the −60 ps and −6 ps PW class laser within a single shot in the Shen Guang II facility. We measured the pulse contrast between the −91 ps and −60 ps PW class laser after expanding the temporal range. The temporal range was 70 ps, with a dynamic range of eight orders of magnitude.

OCIS codes: (320.7090) Ultrafast lasers; (320.7100) Ultrafast measurements; (320.5520) Pulse compression.

http://dx.doi.org/10.1364/AO.55.007538

1. INTRODUCTION

High-energy short-pulse lasers are important in research areas such as particle acceleration, inertial confinement fusion, fast ignition, radiation therapy, and secondary source generation to achieve extreme material states in the laboratory [1–4]. Many high-energy short-pulse lasers have been built worldwide or are under construction. The ultrafast laser systems at the Vulcan and Orion facilities can generate output pulses with a duration of 0.5 ps with an energy of 0.5 kJ [5]. The Omega EP (extended performance) facility at the Laboratory for Laser Energetics in Rochester can generate a pulse of 1–100 ps duration with energy up to 2.6 kJ [6]. The advanced radiographic capability laser system (ARC) at the National Ignition Facility at the Lawrence Livermore National Laboratory can provide eight adjustable pulses of 1–50 ps with energies of 1.7 kJ each [7]. The petawatt (PW) Aquitaine laser at the Laser Mega-Joule facility in Bordeaux can output pulses of 0.5–10 ps of a few kilojoules [8]. The laser for fast ignition experiments (LFEX) laser at the Institute for Laser Engineering in Osaka can provide 10 kJ pulses of 0.5–20 ps [9]. The PW laser at the Shen Guang II (SG-II) facility at Shanghai Institute of Optics and Fine Mechanics can provide 1 kJ pulses of 1–10 ps [10].

The pulse width and contrast are very important for ultrafast lasers. It is possible to measure the pulse width using a streak camera, an autocorrelator, or the frequency-resolved optical gating technique (FROG). The streak camera is a complicated, expensive technique [11] that measures pulse widths ranging from 1 to 100 ps in the OMEGA EP facility. The FROG technique is widely used to analyze spectral width, spectral phase, and pulse width in many ultrafast lasers when the time-bandwidth product is less than ten [12]. Autocorrelation, however, is a more simple, robust technique to measure pulse width [13,14] that is fundamental and acceptable for the usual measurements.

It is possible to measure the pulse contrast using a streak camera, photodiode, or cross-correlator. Tien *et al.* measured the pulse contrast of a laser whose energy, pulse duration, and frequency were 300 μJ 100 fs and 1 Hz, respectively, using a plasma-shuttered streak camera. Its temporal range was −2000 ps–200 ps with a resolution <25 ps and dynamic range of approximately 10^7 [15]. Dorrer *et al.* measured the pulse contrast of the OMEGA EP 1.5 kJ 10 ps lasers in a single shot using the photodiodes. Their measurement technique had a temporal range of −8 ns to −0.5 ns with a resolution of 230 ps and dynamic range above 10^8 [16]. Hillier *et al.* measured the pulse contrast of the 500 J 500 fs Orion lasers using photodiodes. The temporal range was −20 ns to −0.5 ns with a dynamic range of 10^{12} [17]. Wang *et al.* measured the pulse contrast of a 3.5 mJ 35 fs 1 kHz laser measured by a cross-correlator. Its temporal range was −40 ps–10 ps) with a resolution and dynamic range of 0.7 ps and 10^{10}, respectively [18].

Figure 1 shows a schematic diagram of the PW laser system in the SG-II facility. A pulse from a GLX-200 femtosecond laser (Lumentum) with a 200 fs pulse width and 1053 nm wavelength was stretched into a chirped pulse with a 3.2-ns duration by an Offner stretcher. The chirped pulse was first

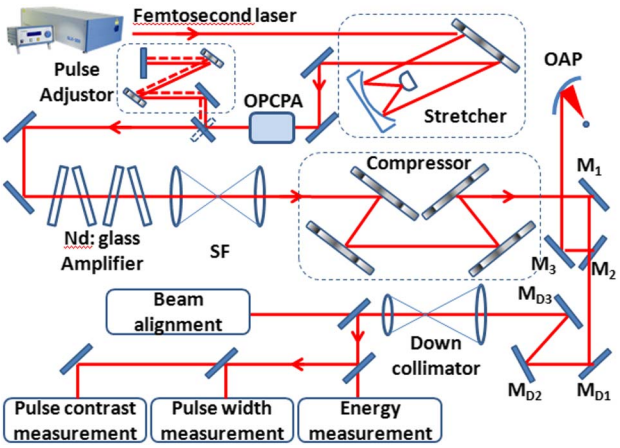

Fig. 1. Schematic diagram of the PW laser at the SG-II facility.

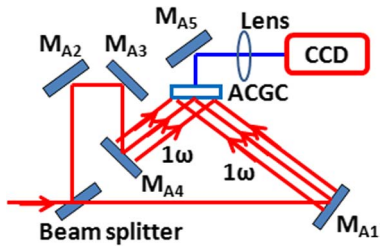

Fig. 2. Schematic diagram of the pulse width measurement in our diagnostics, where M_{A1}, M_{A2}, M_{A3}, M_{A4}, and M_{A5} are mirrors, ACGC is the autocorrelation generation crystal, and CCD is a scientific camera.

amplified to 50 mJ by an optical parametric chirped-pulse amplification (OPCPA) unit [19].

Figure 1 shows a pulse adjustor designed to change the pulse width of the PW laser located between the OPCPA and the Nd:glass amplifier. In the pulse adjustor, a roof prism was used to reflect the chirped pulse back.

The Nd:glass amplifiers then amplified the chirped pulse to 1700 J, its duration was narrowed to 1.7 ns, and its spectral width was shortened from 6.5 to 3.4 nm. We used spatial filters to improve the beam quality and decrease the scattering noise. The 1700 J chirped pulse was compressed using four gratings and strengthened to PW power of 1000 J with duration of 1–10 ps. After being reflected by mirrors M_1, M_2, and M_3, the PW we focused the laser using an off-axis parabolic mirror. The diameter of the focus was 20 μm within 50% of the encircled energy.

We sampled a small part (leakage = 1.5%) of the PW laser by M_2 and it was guided into a diagnostics system. In the diagnostics system, mirrors, M_{D1} and M_{D2}, and an uncoated mirror M_{D3}, reflected the sampled beam. We changed the aperture of the sampled beam from 320 to 40 mm using a down collimator. Beam splitters divided the sampled small-aperture beam into several parts and guided the parts separately into the beam alignment, energy, pulse width, and pulse contrast measurement devices.

2. PULSE WIDTH MEASUREMENT

The pulse width measurement of our diagnostics used a special autocorrelator with a mirror-image configuration, as shown in Fig. 2. The ratio of the input energy guided into the pulse width measurement device to the output energy of the compressor was 5.7×10^{-6}. We first divided the input beam into two parts. The transmitted part of the beam was reflected by a mirror M_{A1} to a β-BaB_2O_4 (BBO) autocorrelation generation crystal (ACGC) measuring 12 mm × 12 mm × 1 mm. The reflected part of the beam was reflected by mirrors (M_{A2}, M_{A3}, and M_{A4}) and sent to the ACGC. Each part had three lines when it arrived at the ACGC to describe the schematic of single-shot measurement.

The angle between these two parts on the ACGC was 55°. We generated a single-shot autocorrelation signal at the ACGC. This signal was reflected by mirror M_{A5}, imaged by a lens, and acquired by a charge-coupled device (CCD, GYD-SG512B12GA, Camyu).

The transmitted part was reflected one time. However, the reflected part was reflected four times. We used this mirror-image configuration to compensate for the defects in the near field or cross-section of the sampled beam. This configuration can robustly decrease the error from the damaged points of the near field in large laser facilities and can improve the measurement accuracy of high-energy PW lasers [20]. After we calibrated the autocorrelator using a 300 fs laser, its temporal range was 18 ps with a resolution of 0.05 ps when we assumed the sampled beam to be a Gaussian pulse.

To improve the accuracy of the pulse width measurement, it was important to do a marginal integration of the two-dimensional (2D) image from the CCD. The optics of the PW laser (the final grating, sampling mirror M_2, and small optics of the down collimator) were vulnerable to damage because of the ultra-high intensity. The damaged points were randomly located in the cross-section of the sampled beam. The marginal integration of the points vertical to the temporal axis in the 2D image is a statistical method that can improve stability in our experiments when the pulse adjustor and compressor are fixed. On the other hand, a cylindrical lens performs the same function as marginal integration when it is set up before the beam splitter.

Figure 3(a) shows how the pulse width of the PW laser was changed by the grating position of the adjustor. The solid line represents the V curve of the pulse width versus the grating position, which is consistent with the results of Kuznetsov *et al.* [21]. The 0.5 ps pulse from the autocorrelator caused the dashed line. The result was very close to the Fourier transmit limitation when the center wavelength was 1053 nm and spectral width was 3.4 nm. There is some noise in the result from the autocorrelator in Fig. 3(a), which is possibly caused by scattering from the environment. It will be subtracted when the measurement software is updated.

The final large grating is vulnerable to damage from the PW laser. Therefore, there are two curves in Fig. 3(b) because the final large grating in the compressor is replaced after damage from the laser–matter interaction experiments. The result of the dashed line in Fig. 3(b) is also acceptable because it is linear.

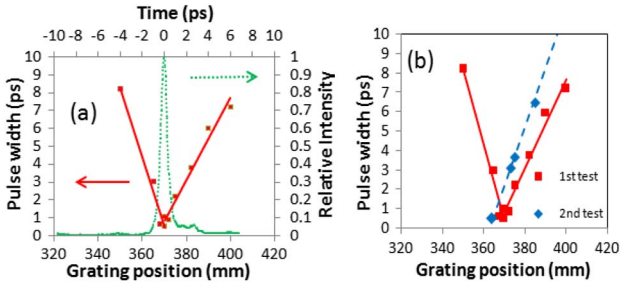

Fig. 3. (a) Pulse width result versus grating position (solid line) and auto-correlation curve of a 0.5-ps pulse (dashed line). (b) Pulse width result versus grating position in the first (solid line) and the second (dashed line) test.

After replacing the last grating, there was a small translation between these two curves caused by a repositioning error after installing and adjusting the final large grating.

Figure 3(b) shows that the performance of the new grating is in good agreement with that of the old one. In addition, the tolerance of the grating replacement can satisfy the requirement of the pulse adjustor from 1–10 ps. Until recently, the sizes of the four gratings in Fig. 1 were 430 mm × 350 mm. They were recently replaced by gratings measuring 1025 mm × 350 mm. We are considering complicated methods of pulse width measurement such as the cross-correlation frequency-resolved optical gating technique to analyze the pulse shape and high-order dispersion in future experiments [22].

3. PULSE CONTRAST MEASUREMENT

The ratio of the input energy guided into the pulse contrast measurement to the output energy of the compressor is also 5.7×10^{-6}. Figure 4 shows the pulse contrast measurement adopts a single-shot cross-correlator with a fiber array configuration as shown in Fig. 4. A beam splitter placed after the attenuator A_1 divided the sampled beam. The transmitted part is used as a pending pulse. The pending pulse was reflected by

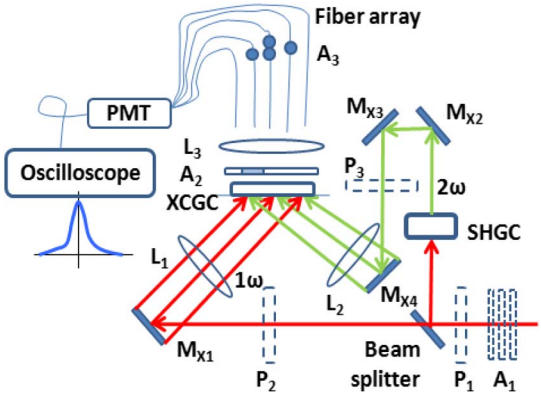

Fig. 4. Schematic diagram of the pulse contrast measurement. M_{X1}, M_{X2}, M_{X3}, and M_{X4} are mirrors; P_1, P_2, and P_3 are removable parallel plates; L_1, L_2, and L_3 are cylindrical lenses; A_1, A_2, and A_3 are attenuators; SHGC is the auto-correlation generation crystal; XCGC is the cross-correlation generation crystal; and PMT is the photomultiplier tube.

the mirror M_{X1}, passed through a cylindrical lens L_1, and arrived at the BBO cross-correlation generation crystal (XCGC) measuring 19 mm × 10 mm × 1 mm in size. The reflected part passed through a second harmonic generation crystal (SHGC) and was used as a gating pulse. The SHGC was a BBO crystal measuring 15 mm × 15 mm × 8 mm. The gating pulse subsequently passed through M_{X2}, M_{X3}, M_{X4}, and the cylindrical lens L_2 before also arriving at the XCGC. After the attenuator A_2, a cylindrical lens L_3 coupled the single-shot cross-correlation signal $I_X(t)$ behind the XCGC into a detector composed of a fiber array, a photomultiplier tube (PMT), and an oscilloscope. The fiber array had 100 fiber channels and included some fiber attenuators A_3 that can be used when needed. The PMT and the fiber array improved the detector's sensitivity [23].

The maximum conversion efficiency of the SHGC and XCGC in our design was approximately 10% and 0.1%, respectively, which means that the energy of the signal will be about 10^{-7} J when the input energy is 1 mJ. The maximum energy of each channel of these 100 fibers is 10^{-9} J. The sensitivity of the PMT is determined by 10 photons of wavelength 351 nm to avoid current noise and was found to be 5.7×10^{-18} J. Therefore, the dynamic range of this measurement is as much as 10^8 because of fine attenuators such as the filters (A_1), coated mirrors (A_2), and fiber attenuators (A_3). The dynamic range may be much higher for a 35 fs laser because of the higher conversion efficiency of the SHGC and XCGC [18]. We carefully calibrated these attenuators before the experiments, with an average error of ±0.13 in log10.

There are two cases in the high dynamic range of pulse contrast measurements. In the first case, we correlated the gating pulse with the prepulse of the pending pulse. There is a large difference between their intensities. The conversion efficiency of the prepulse may be 100%. In the other case, we correlated the gating pulse with the main pulse of the pending pulse. The conversion efficiency of the main pulse in our design was 10%, which is far below 100%, because the intensities of the gating pulse and the main-pulse are closed. Back conversion of one of the two pulses may occur if their intensities are sufficiently high. This phenomenon can be tested by reflection from a parallel plate [24].

An ultra-short pulse $I_1(t)$ can be expressed by a Gaussian function

$$I_1(t) = I_0 \exp\left(-4 \ln 2 \frac{t^2}{\Delta t^2}\right), \quad (1)$$

where Δt is the pulse width and I_0 is the maximum intensity. In this article, we assumed I_0 to be 1.

Figure 4 shows that the input pulse $I_1(t)$ will be followed by a series of pulses with successively decreasing energies after it passes through the parallel plate P_1. The first low-energy pulse can be calculated as

$$I_1'(t) = \exp\left(-4 \ln 2 \frac{t^2}{\Delta t^2}\right) + R \exp\left[-4 \ln 2 \frac{(t+T)^2}{\Delta t^2}\right], \quad (2)$$

where R is the relative intensity of the low-energy pulse and T is the temporal interval between the main pulse and the first low-energy pulse. $T = -2nd/c$ when the thickness of the parallel plate is d and its refractive index is n.

We assumed that the gating pulse underwent a low conversion based on the calibration experiments conducted using the parallel plates P_1, P_2, and P_3 in Fig. 4 [24]. The gating pulse $I_2'(t)$ in cross-correlation can then be expressed as

$$I_2'(t) = \exp\left(-4\ln 2\frac{2t^2}{\Delta t^2}\right) + R^2\exp\left[-4\ln 2\frac{2(t+T)^2}{\Delta t^2}\right]. \quad (3)$$

The cross-correlation signal is

$$\begin{aligned} I_X'(\tau) &= \int I_1'(t)I_2'(t-\tau)\mathrm{d}t \\ &= k_X\exp\left(-4\ln 2\frac{2\tau^2}{3\Delta t^2}\right) \\ &\quad + Rk_X\exp\left[-4\ln 2\frac{2(\tau+T)^2}{3\Delta t^2}\right] \\ &\quad + R^2k_X\exp\left[-4\ln 2\frac{2(\tau-T)^2}{3\Delta t^2}\right] \\ &\quad + R^3k_X\exp\left[-4\ln 2\frac{2\tau^2}{3\Delta t^2}\right]. \end{aligned} \quad (4)$$

In Eq. (4), $k_X = (\pi\Delta t^2/48\ln 2)^{1/2}$, which is the coefficient of cross-correlation.

Comparing Eqs. (2) and (4) shows that the relative intensities of both the peaks at time T is R. There is an additional peak (or artificial peak) at time $-T$ in the cross-correlation, with a relative intensity of R^2. These features can be used to verify the pulse contrast results.

We inserted a parallel plate of 3.11 mm thick H-K9L glass (CDGM Glass) at P_1, P_2, and P_3 for pulse contrast measurements separately, as shown in Fig. 4. The refractive index was 1.517 at 1053 nm. The reflectivity of each surface of the parallel plate was 4% because they are uncoated. Then, the relative intensity of R is 1.6×10^{-3}. We verified the error of nonlinear efficiency versus different input pulse powers by changing the number of filters at A_1 [24]. The maximum error was 0.54 in log10, and the average error was 0.29 in log10. We then assumed the error of nonlinear efficiency as ±0.29 in log10. This method was helpful to confirm the high dynamic range in pulse contrast measurements.

We verified the performance of the pulse contrast measurement by a 0.5 mJ 300 fs 1 Hz laser with these attenuators and the parallel plate. A peak in the ratio of 1.5×10^{-6} (−5.84 in log10) emerged at 31.5 ps of the solid line (single-shot result I) in Fig. 5 when the parallel plate was inserted at P_1, as shown in Fig. 4. There was no peak at the same position in the dashed line (single-shot result II) of Fig. 5 when the parallel plate was removed. The chain-like line in Fig. 5 was the result measured by Sequoia (Amplitude Technologies), which is widely used in pulse contrast measurement for repetition pulses [25].

There are three additional peaks in the results of the pulse contrast measurement for a single shot pulse compared with the Sequoia result. They can be observed at −60 ps, −43.5 ps, and −28.5 ps, and are caused by the extremely small reflectivity of the back surfaces. We determined the results of the pulse contrast measurement in the regions of −6 ps to −1.5 ps and 1.5 ps to 10 ps by interpolation because the original data is hard to interpret because of the extremely high attenuation. This issue means that no not genuine measurement data exists. There was a small difference at −10 ps in Fig. 5 because of the random variation of the laser, which can be distinguished by the two single-shot results. The results from the Sequoia are an average of 10 data points at each time position, thus preventing us from observing the random variation of the laser. We have shown that a dynamic range of 10^8 (8 in log10) was reliable for pulse contrast measurements using the uncoated parallel plate. The total temporal range was −60 ps to 10 ps with a resolution of 0.75 ps after calibration.

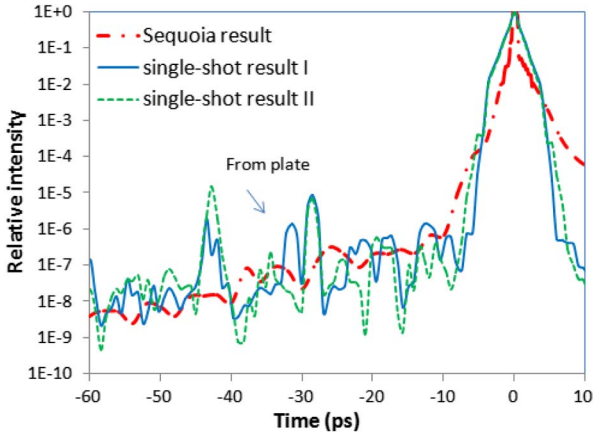

Fig. 5. Performance test of the pulse contrast measurement.

Figure 6 shows that the pulse contrast of the PW class laser was measured when the pulse width was 0.5 ps and pulse energy was 175 J, which means that the energy of the pulse contrast measurement was 1 mJ with a total attenuation of 5.7×10^{-6}. The power of the sampled beam for the PW laser was 2 GW, which was close to that of the sampled beam for the femtosecond laser. Thus, we can use the results in Fig. 5 as a reference for the PW laser.

The solid line in Fig. 6(a) shows the pulse contrast of a single-shot pulse. The reference is indicated by the dashed line in Fig. 6(a), which is from the single-shot result II in Fig. 5. The minimums of the two results in Fig. 6(a) are both 10^{-8}. We have proven that the dynamic range of the pulse contrast measurement is 10^8 when the input power is approximately 2 GW. We observed greater noise in the results obtained by the PW laser compared to that observed in the results of the low-energy laser.

The additional peak did not emerge at time −31.5 ps when an uncoated parallel plate was inserted at P_1. However, it appeared when another coated parallel plate, the reflectivity of one

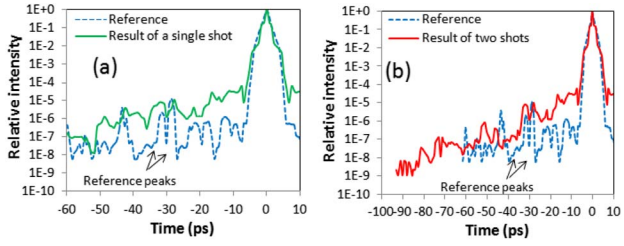

Fig. 6. Experimental data of the pulse contrast measurement in the PW class laser by (a) one shot (a) and (b) two shots.

of whose surfaces was 0.08, was inserted. Then, the additional peak ratio at time −31.5 ps was 1×10^{-5} (5 in log10).

We moved the time delay of the pulse contrast measurement (M_3 and M_4 in Fig. 1) from 9.55 to 14.21 mm for another single shot of the PW laser. The optical path was 31 ps in air. We changed the temporal range from between −60 ps and 10 ps to −91 ps and −21 ps. These two results can be connected together in an expanding window of −91 ps to 10 ps based on the reference peaks at time −31.5 ps and −28.5 ps, as shown in Fig. 6(b).

There is some difference at −60 ps and −40 ps between Figs. 6(a) and 6(b). We observed a peak at −5 ps in a previous measurement [24]. Noise from −60 ps to −10 ps decreased significantly to 10^{-8} after we attenuated the peak at −5 ps. We can conclude that the ratio of the scattering noise to peak is 10^{-4}. The scattering noise then is on the order of 10^{-9} in the range of −91 ps to 21 ps because the maximum peak is 10^{-5} in this range. Therefore, the expanding window contains less noise than the single window with the main pulse. In the future, the reflection of the back surface and scattering noise in the single window should be considered more carefully.

The PW class laser in the SG-II facility has a pulse contrast of 10^8 (8 in log10) before −81.75 ps, 10^7 (7 in log10) before 72.75 ps, 10^6 (6 in log10) before −51 ps, and 3.3×10^4 (4.5 in log10) at −10 ps.

4. CONCLUSION

We carefully performed a temporal characterization of the PW laser at the SG-II facility using pulse width and pulse contrast measurements. The pulse width measurement showed that a V curve could be described by a special autocorrelator with a mirror image configuration, which can compensate for the near-field defects in large laser facilities. Additionally, the pulse width measurement performs well after grating replacements. The dynamic range of the pulse contrast measurement was eight orders of magnitude, which we calibrated using parallel plates and a Sequoia. The temporal range was −60 ps to 10 ps under a single shot. This measurement described the pulse contrast of the PW laser between −91 ps and −6 ps within two shots of the laser pulse by moving the time delay.

Funding. National Natural Science Foundation of China (NSFC) (11204330).

Acknowledgment. We thank Professors Liejia Qian, Yuxin Leng, and Guang Xu for their experimental assistance.

REFERENCES

1. S. P. D. Mangles, C. D. Murphy, Z. Najmudin, A. G. R. Thomas, J. L. Collier, A. E. Dangor, E. J. Divall, P. S. Foster, J. G. Gallacher, C. J. Hooker, D. A. Jaroszynski, A. J. Langley, W. B. Mori, P. A. Norreys, F. S. Tsung, R. Viskup, B. R. Walton, and K. Krushelnick, "Monoenergetic beams of relativistic electrons from intense laser-plasma interactions," Nature **431**, 535–538 (2004).
2. L. Robson, P. T. Simpson, R. J. Clarke, K. W. D. Ledingham, F. Lindau, O. Lundh, T. McCanny, P. Mora, D. Neely, C.-G. Wahlstrom, M. Zepf, and P. McKenna, "Scaling of proton acceleration driven by petawatt–laser–plasma interactions," Nat. Phys. **3**, 58–62 (2007).
3. H. Cai, S. Wu, J. Wu, M. Chen, H. Zhang, M. He, L. Cao, C. Zhou, S. Zhu, and X. He, "Review of the current status of fast ignition research at the IAPCM," High Power Laser Sci. Eng. **2**, e6 (2014).
4. C. Danson, D. Hillier, N. Hopps, and D. Neely, "Petawatt class lasers worldwide," High Power Laser Sci. Eng. **3**, e3 (2015).
5. N. Hopps, C. Danson, S. Duffield, D. Egan, S. Elsmere, M. Girling, E. Harvey, D. Hillier, M. Norman, S. Parker, P. Treadwell, D. Winter, and T. Bett, "Overview of laser systems for the Orion facility at the AWE," Appl. Opt. **52**, 3597–3607 (2014).
6. J. D. Zuegel, S. Bahk, J. Bromage, C. Dorrer, R. Earley, T. J. Kessler, B. J. Kruschwitz, S. F. B. Morse, D. N. Maywar, J. B. Oliver, J. Qiao, A. L. Right, A. W. Schmid, M. J. Shoup III, L. J. Waxer, and J. H. Kelly, "Novel laser and diagnostic technologies for the OMEGA EP high-energy petawatt laser," Rev. Laser Eng. **37**, 437–442 (2009).
7. J. M. Di Nicola, S. T. Yang, C. D. Boley, J. K. Crane, J. E. Heebner, T. M. Spinka, P. Arnold, C. P. J. Barty, M. W. Bowers, T. S. Budge, K. Christensen, J. W. Dawson, G. Erbert, E. Feigenbaum, G. Guss, C. Haefner, M. R. Hermann, D. Homoelle, J. A. Jarboe, J. K. Lawson, R. Lowe-Webb, K. McCandless, B. McHale, L. J. Pelz, P. P. Pham, M. A. Prantil, M. L. Rehak, M. A. Rever, M. C. Rushford, R. A. Sacks, M. Shaw, D. Smauley, L. K. Smith, R. Speck, G. Tietbohl, P. J. Wegner, and C. Widmayer, "The commissioning of the advanced radiographic capability laser system experimental and modeling results at the main laser output," Proc. SPIE **9345**, 93450I (2015).
8. J. L. Miquel, D. Batani, and N. Blanchot, "Overview of the laser mega joule (LMJ) facility and PETAL project in France," Rev. Laser Eng. **42**, 131–136 (2014).
9. H. Shiraga, S. Fujioka, M. Nakai, T. Watari, H. Nakamura, Y. Arikawa, H. Hosoda, T. Nagai, M. Koga, and H. Kikuchi, "Fast ignition integrated experiments with Gekko and LFEX lasers," Plasma Phys. Contr. F. **53**, 124029 (2011).
10. T. Wang, G. Xu, Y. Dai, Z. Lin, Y. Gu, and J. Zhu, "A petawatt beamline on SG-II-U laser system," in *Conference on Lasers and Electro-Optics Europe and 11th European Quantum Electronics Conference (CLEO/EQEC)* (2009), paper 5196348.
11. J. Bromage, J. D. Zuegel, S. W. Bahk, D. S. Vickery, L. J. Waxer, D. Irwin, V. Bagound, R. Boni, M. D. Moore, R. Jungquist, and C. Stoeckl, "High-intensity laser diagnostics for OMEGA EP," J. Phys. IV France **133**, 705–707 (2006).
12. J. Cohen, D. Lee, V. Chauhan, P. Vaughan, and R. Trebino, "Highly simplified device for measuring the intensity and phase of picosecond pulses," Opt. Express **18**, 17484–17497 (2010).
13. F. Salin, P. Georges, G. Roger, and A. Brun, "Single-shot measurement of a 52-fs pulse," Appl. Opt. **26**, 4528–4531 (1987).
14. R. A. Ganeev, F. S. Ganikhanov, I. G. Gorelik, A. A. Dakhin, D. G. Kunin, T. Usmanov, and A. V. Zinoviev, "Laser pulse duration measurements in the range of 0.2 to 50 picosecond," Opt. Commun. **114**, 432–434 (1995).
15. A. Tien, M. Nantel, G. Mourou, D. Kaplan, and M. Bouvier, "High-dynamic-range laser-pulse-contrast measurement with a plasma-shuttered streak camera," Opt. Lett. **22**, 1559–1561 (1997).
16. C. Dorrer, D. Irwin, A. Consentino, and J. Qiao, "Control measurements of kilojoule laser pulses at the Omega EP laser facility," in *Conference on Lasers and Electro-Optics (CLEO/QELS)* (2010), paper JThE117.
17. D. I. Hiller, S. Elsmere, M. Girling, N. Hopps, D. Hussey, S. Parker, P. Treadwell, D. Winter, and T. Bett, "Contrast enhancements to petawatt laser using short pulse optical parametric amplifiers and frequency doubling," Appl. Opt. **53**, 6938–6943 (2014).
18. Y. Wang, J. Ma, J. Wang, P. Yuan, G. Xie, X. Ge, F. Liu, X. Yuan, H. Zhu, and L. Qian, "Single-shot measurement of >1010 pulse contrast for ultra-high peak-power lasers," Sci. Rep. **4**, 3818 (2014).
19. G. Xu, T. Wang, Z. Li, Y. Dai, Z. Lin, Y. Gu, and J. Zhu, "1 kJ petawatt laser system for SG-II-U program," Rev. Laser Eng. **36** (suppl), 1172–1175 (2008).
20. X. Ouyang, J. Ma, L. Yang, S. Tang, C. Liu, Y. Peng, L. Qian, B. Zhu, J. Zhu, and Z. Lin, "Accuracy of single-shot autocorrelation measurements of petawatt laser pulses," Appl. Opt. **51**, 3989–3994 (2012).
21. M. Kuznetsov, J. M. Wiesenfeld, and L. R. Radzihovsky, "Compression of picosecond pulses from diode lasers using a modified grating-pair compressor," Opt. Lett. **15**, 180–182 (1990).

22. T. C. Wong and R. Trebino, "Single-frame measurement of complex laser pulses tens of picoseconds long using pulse-front tilt in cross-correlation frequency-resolved optical gating," J. Opt. Soc. Am. B **30**, 2781–2786 (2013).
23. D. Zhang, L. Qian, P. Yuan, H. Zhu, S. Wen, and C. Xu, "Fiber-array-based detection scheme for single-shot pulse contrast characterization," Opt. Lett. **33**, 1969–1971 (2008).
24. X. Ouyang, D. Liu, B. Zhu, J. Zhu, and J. Zhu, "Diagnostics of pulse contrast for petawatt laser in SGII," Proc. SPIE **9345**, 93450R (2015).
25. H. Liebetrau, M. Hornung, A. Seidel, M. Hellwing, A. Kessler, S. Keppler, F. Schorcht, J. Hein, and M. C. Kaluza, "Ultra-high contrast frontend for high peak power fs-laser at 1030 nm," Opt. Express **22**, 24776–24786 (2014).